

Multi-site Organ Segmentation with Federated Partial Supervision and Site Adaptation

Pengbo Liu^{1†}, Mengke Sun^{2,3†}, and S. Kevin Zhou^{1,3*}

¹Center for Medical Imaging, Robotics, Analytic Computing & Learning (MIRACLE), School of Biomedical Engineering & Suzhou Institute for Advanced Research, University of Science and Technology of China, Suzhou 215123, China

²Beijing UCAS Space Technology Co., Ltd., Beijing, China.

³Key Lab of Intelligent Information Processing of Chinese Academy of Sciences (CAS), Institute of Computing Technology, CAS, Beijing 100190, China

*Corresponding author. Email: skevinzhou@ustc.edu.cn

[†]These authors contributed equally to this work.

Abstract

Objective and Impact Statement: Accurate organ segmentation is critical for many clinical applications at different clinical sites, which may have their specific application requirements that concern different organs. *Introduction:* However, learning high-quality, site-specific organ segmentation models is challenging as it often needs on-site curation of a large number of annotated images. Security concerns further complicate the matter. *Methods:* The paper aims to tackle these challenges via a two-phase aggregation-then-adaptation approach. The first phase of federated aggregation learns a single multi-organ segmentation model by leveraging the strength of ‘bigger data’, which are formed by (i) aggregating together datasets from multiple sites that with different organ labels to provide partial supervision, and (ii) conducting partially supervised learning without data breach. The second phase of site adaptation is to transfer the federated multi-organ segmentation model to site-specific organ segmentation models, one model per site, in order to further improve the performance of each site’s organ segmentation task. Furthermore, improved marginal loss and exclusion loss functions are used to avoid ‘knowledge conflict’ problem in a partially supervision mechanism. *Results and Conclusion:* Extensive experiments on five organ segmentation datasets demonstrate the effectiveness of our multi-site approach, significantly outperforming the site-per-se learned models and achieving the performance comparable to the centrally learned models.

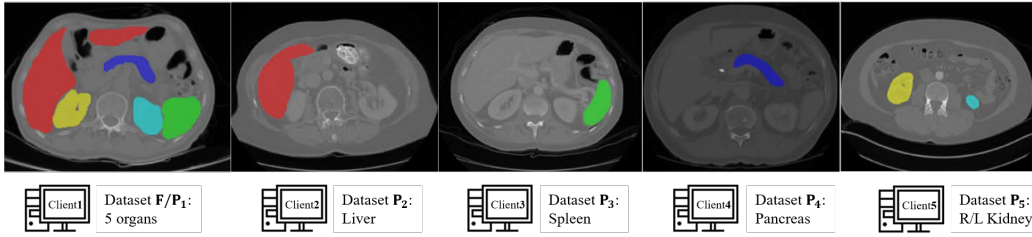


Figure 1: CT images of different partially labeled datasets for different tasks at different clinical sites. The red, green, blue, yellow, and cyan color represent liver, spleen, pancreas, right kidney, and left kidney, respectively.

1 Introduction

Accurate organ segmentation is critical for many clinical applications [1, 2] at different clinical sites, which may have their specific application requirements that concern different organs. But in the medical images scenario, curating large-scale annotated datasets even within the site is a challenging job, which is expensive and time-consuming. As a result, the scale of the currently labeled datasets is usually limited, thereby limiting the performance of models learned site per se.

Recently there is a growing interest in learning multi-organ segmentation models from a union of datasets collected from multiple sites, thereby leveraging the strength of ‘bigger data’ for improved performances. Because different sites have site-specific organ labels (as shown in Fig. 1), forming a partial supervision condition in aggregation. In other words, most of these datasets are partially annotated in terms of full labeling, which is also a bottleneck in the field of multi-organ segmentation research. We can not directly deploy fully supervised segmentation methods on this kind of dataset due to ‘knowledge conflict’ [3] problem: *The foreground in one dataset becomes background in another dataset.* Although some existing studies [4–10] have solved this problem, making use of these datasets together, they all conduct model learning centrally. In reality, due to ethical and privacy issues, data cannot be shared among different institutions, nor are data among different departments of the same institution. Data often exists in the form of isolated islands, a phenomenon that is more common in the medical domain. Therefore, traditional centralized deep learning methods encounter serious challenges because the data are fragmented into many different sites. At the same time, more and more attention has been paid to the security and privacy of the data, especially the security and privacy of medical image data. Many countries have promulgated relevant data security protection laws, such as the EU’s General Data Protection Regulation (GDPR) [11]. The above issues make the collection and the use of large-scale datasets for machine learning more difficult.

The timely emergency of federated learning (FL) technology alleviates the data privacy issue [12]. FL allows that data do not leave their original institution or organization, and train the global federated model collaboratively and effectively under the coordination of a central parameter server. During the standard training process of the global federated model, each local client firstly downloads federated model parameters from the central server and trains the model parameters locally based on local data. Next, the locally trained model parameters for each client are sent back to the central server. Then, the central server aggregates model parameters from all clients to get a better global

federated model. The final global federated model is obtained through multiple iterations of the above steps. In this process, all data in each client never leave the local storage, but the task in each client *should be same*. In [13], the authors curate partially labeled datasets by constructing different encoders for different tasks in federated form, which limits the scalability of this method as the clients and tasks increases. Directly encoding multi-task into a single network via FL failed [14] because of ‘knowledge conflict’ problem. Therefore, the representational capabilities of a single network are far from being exploited. In this work, we attempt to bridge the gap by proposing a two-stage approach to multi-site organ segmentation. The first stage of federated aggregation is to learn *a unified single multi-organ* segmentation model in a federated fashion under *the condition of partial supervision*, with ‘knowledge conflict’ problem solved.

The goal of multi-site organ segmentation requires learning site-dependent, and application-specific organ segmentation models. Directly using the federated multi-organ segmentation model as the multi-site model is not ideal as it is known that the performance of a federated model is inferior to that of a centrally learned model for the same task. Furthermore, there is a domain shift problem among different sites as they use different scanners and protocols for data acquisition. To accommodate such a domain shift, we propose the second stage of site adaptation, which transfers the federated multi-organ segmentation model to a site-dependent, application-specific organ segmentation model in order to further improve the performance of each organ segmentation task per site.

Our main contributions can be summarized as:

- We make *the first attempt* in the literature to merge multiple partially labeled datasets of different tasks from different sources into *a unified single model* via federated learning method, fusing different tasks in different clients to one single federated model on the central server and also solving the privacy issue.
- We design a new combination of loss functions based on marginal loss and exclusion loss [9] to solve the ‘knowledge conflict’ problem and improve the performance of partially supervised multi-organ segmentation.
- We transfer the features of the federated model to a local site-dependent, application specific organ segmentation model in order to alleviate the domain gap and further improve the performance of each local model, thereby realizing multi-site organ segmentation.
- Our extensive experiments verify the effectiveness of our approach on multisite organ segmentation scenario, getting state-of-the-art (SOTA) performance compared with the upper bound method [9], which can centrally access all datasets during training, and surpassing the performance of models trained separated on each local site by a large margin.

The rest of this paper is organized as follows: In Section 2, extensive experiments are conducted to demonstrate the effectiveness of the method. Section 3 presents our conclusions. Section 4 presents the details of the method.

Table 1: The overview of five benchmark datasets used in our experiments.

Datasets	Modality	# training data	# testing data	Annotated organs	Mean spacing (z,y,x) in mm
F (P_1)	CT	24	6	Fully annotated	(3.00, 0.76, 0.76)
P_2	CT	105	26	Liver	(1.00, 0.77, 0.77)
P_3	CT	33	8	Spleen	(1.60, 0.79, 0.79)
P_4	CT	225	56	Pancreas	(2.50, 0.80, 0.80)
P_5	CT	186	24	Left & right kidneys	(0.80, 0.78, 0.78)

2 Results

We conduct a series of experiments to verify the following assumptions: (i) The different combination of loss functions plays an important role in our Partially Supervised Multi-Organ Segmentation (PSMOS) task, either non-federated learned (*aka* centrally learned, non-FL PSMOS) or federated learned (FL PSMOS). (ii) FL PSMOS can achieve a comparable performance to non-FL PSMOS. (iii) Site adaptation at each local clinical site makes the segmentation performance better.

2.1 Experiment Settings

2.1.1 Datasets and evaluation metrics

In our experiments, for fair comparison with MargExc [9] that is a centrally-learned multi-organ segmentation approach as our baseline model, we use the same five abdominal datasets with different annotation of different organs used in MargExc, including liver, spleen, pancreas, left kidney, and right kidney. The details of these datasets, F or P_1 (with full label), P_2 (with liver label only), P_3 (with spleen label only), P_4 (with pancreas label only), P_5 (with labels of left and right kidneys), are shown in Table 1.

As the prominent and robust performance of nnUNet [15] in medical image segmentation tasks, our multi-organ segmentation models are all constructed based on it. We preprocess all datasets to a unified spacing ($2.41 \times 1.63 \times 1.63$) and normalize them with mean and std of 90.9 and 65.5, respectively. Due to the GPU memory limitation, we crop 3D patches of size [80, 160, 128] from 3D volumes during training. And we only keep the patches whose target area is larger than 33% for the stability of model training. There are two patches per iteration and 250 iterations per epoch in our experiments. The initial learning rate of the model is 0.01. Whenever the loss reduction is less than 0.001 in consecutive 10 epochs, the learning rate decays by 20%. All other remaining hyper-parameters, including settings for data augmentation, follow the default settings of the nnUNet [15].

We use the Dice coefficient (DC) and 95th percentile Hausdorff distance (HD95) to evaluate our results. The higher the DC or the smaller the HD95, the better the segmentation model.

2.1.2 Loss functions in training of non-FL PSMOS

In this section, we evaluate the influence of different combinations of loss functions in PSMOS task, and take non-FL format as an example. The training process starts from training the model for 120 epochs using only the fully-annotated dataset F , which provides a good start for the whole training process of multi-organ segmentation model. Then it continues the training for 380 epochs using both

the fully-labeled dataset F and the other four partially-labeled datasets, $P_{2,3,4,5}$. The loss functions used in our experiments include Dice Loss [16], Lovasz Loss [17], Cross Entropy Loss [16], Top-K Loss [18] and Focal Loss [19]. According to whether the input CT image is fully annotated or not, we adopt different version of corresponding loss functions. Specifically, for fully-labeled data in F , we use conventional loss functions directly; for partially-labeled data in $P_{2,3,4,5}$, we use the marginal and exclusion variants of the Dice Loss, Lovasz Loss, Cross Entropy Loss, Top-K Loss and Focal Loss. The details please refer to Section 4.

2.1.3 Training of FL PSMOS

We simulate the server (S) with one RTX Titan GPU and terminal clients ($T_n, n \in \{1, \dots, 5\}$) with five RTX Titan GPUs. The server owns the pre-trained multi-organ segmentation model, $\Phi_{pretrained}^m$, which is obtained by training the 3D nnUNet [15] for 120 epochs with the fully-labeled dataset F , which is owned by the client T_1 . Other client T_n owns partially-annotated dataset $P_n, n \in \{2, \dots, 5\}$. All clients share the same neural network structure (i.e., 3D nnUNet [15]) and hyper-parameters.

Finally, we train the following models for comparison.

- Φ_{Mix}^m : the non-FL multi-organ segmentation model trained centrally in one site;
- Φ_{Fed}^m : the FL multi-organ segmentation model trained in the form of federated learning;
- Φ_F^m : the multi-organ segmentation model trained only with the fully annotated dataset F ;
- $\Phi_{P_n}^b$: the binary segmentation model trained with the partially annotated dataset P_n ($n \in \{2, 3, 4\}$);
- $\Phi_{P_5}^t$: The ternary segmentation model trained with the partially labeled dataset P_5 .

The non-FL models $\Phi_F^m, \Phi_{P_2}^b, \Phi_{P_3}^b, \Phi_{P_4}^b$ and $\Phi_{P_5}^t$ use a combination of conventional Dice Loss [16], Cross Entropy Loss [16], and Lovasz Loss [17]; the non-FL model Φ_{Mix}^m and FL model Φ_{Fed}^m use a mix of conventional and marginal& exclusion variants of Dice, Cross Entropy, and Lovasz loss functions [9]. The details of training the FL PSMOS models, please refer to Section 4.

2.1.4 Adapting the FL model to local sites

After federated learning, we obtain a FL PSMOS model, Φ_{Fed}^m , which is trained utilizing all data from different clients, without private information leakage. Then we adapt Φ_{Fed}^m to each clinical site to suit their own task. Since there are three ways of fine-tuning for site adaptation, we obtain three models: Φ_{FTA} (fine-tuning both the encoder and decoder), Φ_{FTB} (fine-tuning only the decoder), and Φ_{FTC} (fine-tuning only the encoder).

2.2 Results

2.2.1 The results of non-FL PSMOS model

The performance of non-FL PSMOS models with different combinations of loss functions on F and $P_{2,3,4,5}$ datasets is shown in Table 2. We observe that the centrally trained Φ_{Mix}^m achieves the best

Table 2: The performance of the non-FL (aka centrally learned) multi-organ segmentation model Φ_{Mix}^m on F and P_* datasets, using different combinations of loss functions. $L_*^{m\&e}$ means the combination of marginal * loss and exclusion * loss ($L_*^m + L_*^e$).

Different combinations of loss functions					[F] Liver		[F] Spleen		[F] Pancreas		[F] L Kidney		[F] R Kidney		Mean	
$L_{Dice}^{m\&e}$	$L_{Lovasz}^{m\&e}$	$L_{CE}^{m\&e}$	$L_{Topk}^{m\&e}$	$L_{Focal}^{m\&e}$	DC	HD95	DC	HD95	DC	HD95	DC	HD95	DC	HD95	DC	HD95
✓		✓			.969	1.71	.943	1.47	.835	3.27	.945	1.58	.950	1.35	.928	1.88
✓				✓	.972	1.77	.935	1.62	.826	4.43	.944	1.40	.949	1.22	.925	2.09
✓	✓				.971	1.59	.931	1.60	.826	4.67	.948	1.37	.953	1.21	.926	2.09
		✓			.969	1.65	.940	1.50	.834	3.92	.943	1.39	.949	1.24	.927	1.94
✓			✓	✓	.970	1.91	.945	1.37	.833	3.79	.943	1.34	.951	1.95	.928	3.71
✓			✓	✓	.972	1.59	.947	1.36	.824	6.71	.948	1.37	.953	1.28	.929	2.46
✓	✓		✓		.972	1.79	.946	1.43	.849	3.04	.950	1.37	.948	1.28	.933	1.78

Different combinations of loss functions					[P ₂] Liver		[P ₃] Spleen		[P ₄] Pancreas		[P ₅] L Kidney		[P ₅] R Kidney		Mean	
$L_{Dice}^{m\&e}$	$L_{Lovasz}^{m\&e}$	$L_{CE}^{m\&e}$	$L_{Topk}^{m\&e}$	$L_{Focal}^{m\&e}$	DC	HD95	DC	HD95	DC	HD95	DC	HD95	DC	HD95	DC	HD95
✓		✓			.941	9.57	.975	1.05	.790	6.08	.972	1.64	.966	15.61	.929	6.79
✓				✓	.935	13.30	.970	1.07	.778	6.13	.971	4.26	.957	16.02	.922	8.16
✓			✓		.928	15.23	.972	1.10	.779	6.15	.954	2.89	.949	15.48	.916	8.17
	✓		✓		.940	13.11	.969	1.08	.788	6.29	.972	3.56	.954	15.38	.925	7.88
✓			✓	✓	.942	13.12	.975	1.05	.786	6.05	.970	3.20	.968	15.40	.928	8.74
✓			✓	✓	.937	9.78	.972	1.05	.783	6.26	.970	5.06	.950	17.41	.922	8.95
✓	✓		✓		.948	6.54	.974	1.05	.795	5.08	.974	1.44	.969	14.57	.932	6.49

Table 3: Comparison with state-of-the-art results. The Training/Testing set split of ours is the same as compared methods. The non-FL, FL and FT means centrally trained, federated trained, and adapted or fine-tuned model, respectively.

Methods	[F&P ₂] Liver		[F&P ₃] Spleen		[F&P ₄] Pancreas		[F&P ₅] L Kidney		[F&P ₅] R Kidney		Mean	
	DC	HD95	DC	HD95	DC	HD95	DC	HD95	DC	HD95	DC	HD95
PaNN [7]	.961	2.99	.941	11.21	.767	7.04	.919	3.76	.943	1.43	.906	5.29
PIPO [8]	.940	10.13	.919	11.54	.772	6.08	.948	4.56	.962	1.17	.908	6.69
MargExc [9]	.955	5.64	.959	1.26	.813	4.68	.959	1.61	.958	8.48	.929	4.33
Φ_{Mix}^m (Ours, non-FL)	.960	4.17	.960	1.24	.822	4.06	.962	1.41	.959	7.93	.933	3.76
Φ_{Fed}^m (Ours, FL)	.952	4.76	.952	1.77	.814	5.89	.952	2.56	.949	9.03	.924	4.80
Φ_{FTB} (Ours, FT)	.957	4.00	.958	1.94	.816	5.24	.959	2.34	.953	8.36	.929	4.38

performance with the combination of $\{L_{Dice}^m, L_{CE}^m, L_{Lovasz}^m, L_{Dice}^e, L_{CE}^e, L_{Lovasz}^e\}$. The average DC and HD95 reach 0.933 and 1.78, respectively, on the fully annotated dataset F , and 0.932 and 6.49, respectively, on the partially-annotated dataset P_n , ($n \in \{2, 3, 4, 5\}$). In the first four rows of two tables in Table 2, which are the combinations of two loss functions. Based on the basic combination of Dice and CE loss in MargExc [9], we try different combinations and find that Dice and CE loss are indeed the best combination. Based on this discovery, we add other loss functions separately and find that $\{L_{Dice}^{m\&e}, L_{CE}^{m\&e}, L_{Lovasz}^{m\&e}\}$ is the best combination scheme in the end, which indicate that improve the combination of loss functions plays an important role in the PSMOS task. In particular, the optimized loss function have a significant improvement on small and irregular organs such as the pancreas.

Compared with other SOTA methods as shown in Table 3, our model Φ_{Mix}^m achieves better performance. Specifically, the average DC of the proposed method using the above-mentioned loss function combination is 2.7%, 2.5% and 0.4% higher than that of PaNN [7], PIPO [8], and MargExc [9], respectively. At the same time, our method also greatly reduces the HD95, which is 28.9%, 43.8%, and 13.2% less than the other three methods, respectively. From the visualization results shown in Fig. 2, we can also perceive that our method works better, especially on small and irregular organ such as pancreas, which have finer segmentation results compared with other SOTA methods.

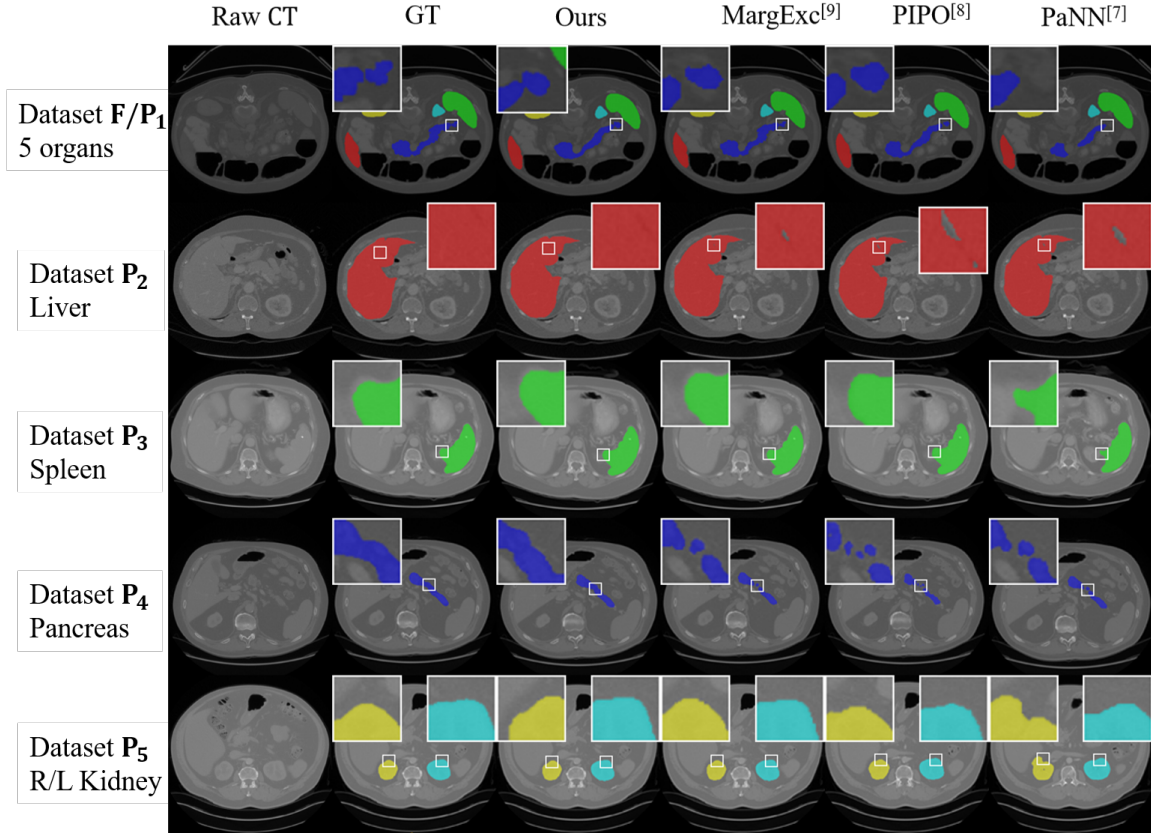


Figure 2: Visualization of the segmentation results of our proposed method and other SOTA methods.

2.2.2 The results of FL PSMOS model

In FL setting, we treat non-FL PSMOS model (Φ_{Mix}^m) as upper bound for comparison. Because Φ_{Mix}^m is trained centrally in one site, which is the most ideal scenario for training. In Table 4, the average DC of Φ_{Mix}^m on F and $P_n, n \in \{2, 3, 4, 5\}$ are 0.933 and 0.932, respectively, and HD95 is 1.78 and 5.74, respectively.

When we do not aggregate these partially labeled datasets together, there is no data leakage problem either, but the performance of the segmentation models suffer greatly due to the greatly reduced scale of the dataset. For instance, in T_1 , Φ_F^m is trained based on its own dataset F and has no access to other dataset in other clients. The performance of Φ_F^m on its own dataset F reaches 0.905 and 3.71 for DC and HD95, respectively. Similarly, $\Phi_{P_n}^b, n \in \{2, 3, 4\}$ and $\Phi_{P_5}^t$ are also trained on their own partially labeled datasets $P_n, n \in \{2, 3, 4, 5\}$, achieving average DC and HD95 of 0.894 and 8.02, respectively. The performances of these models trained separately on their own dataset all have a large gap compared with Φ_{Mix}^m .

When we involve FL, Φ_{Fed}^m can be trained on all datasets from all clients without data leakage, aggregating knowledge from all data that can be accessed. And in our setting, the tasks of different clients are different. We also aggregate these tasks into a single multi-organ segmentation model,

Table 4: The segmentation performance comparison between models trained separately (Φ_F^m , $\Phi_{P_n}^*$), centralized (Φ_{Mix}^m) and federated (Φ_{Fed}^m).

Methods	[F] Liver		[F] Spleen		[F] Pancreas		[F] L Kidney		[F] R Kidney		Mean	
	DC	HD95	DC	HD95	DC	HD95	DC	HD95	DC	HD95	DC	HD95
Φ_F^m	.950	2.94	.925	4.35	.817	6.02	.918	2.47	.915	2.79	.905	3.71
Φ_{Fed}^m (Ours)	.965	2.41	.939	2.33	.840	4.79	.938	1.65	.936	1.50	.924	2.54
Φ_{Mix}^m (Ours, Upper bound)	.972	1.79	.946	1.43	.849	3.04	.950	1.37	.948	1.28	.933	1.78

Methods	[P ₂] Liver		[P ₃] Spleen		[P ₄] Pancreas		[P ₅] L Kidney		[P ₅] R Kidney		Mean	
	DC	HD95	DC	HD95	DC	HD95	DC	HD95	DC	HD95	DC	HD95
$\Phi_{P_2}^b$.914	7.02	-	-	-	-	-	-	-	-	-	-
$\Phi_{P_3}^b$	-	-	.955	1.41	-	-	-	-	-	-	.894	8.02
$\Phi_{P_4}^b$	-	-	-	-	.747	7.63	-	-	-	-	-	-
$\Phi_{P_5}^b$	-	-	-	-	-	-	.928	5.57	.926	18.50	-	-
Φ_{Fed}^m (Ours)	.938	7.10	.965	1.21	.788	6.99	.966	3.47	.961	16.56	.924	7.06
Φ_{Mix}^m (Ours, Upper bound)	.948	6.54	.974	1.05	.795	5.08	.974	1.44	.969	14.57	.932	5.74

Table 5: Experimental results under different federated learning hyper-parameters settings.

Model	Different training setting			Results		
	Client iteration	Global round (epoch)	Total iteration	Dice	HD95	Training time (h)
Φ_{Fed} V1	25	4,000		.895	5.44	94
Φ_{Fed} V2	50	2,000	100,000	.924	4.80	89
Φ_{Fed} V3	100	1,000		.919	4.61	82
Φ_{Mix} (non-FL)	250	500	125,000	.933	3.76	75

and the ‘knowledge conflict’ problem between different tasks in partially annotated datasets is also solved through the combination of loss functions discussed in Section 2.2.1. In Table 4, Φ_{Fed}^m achieves 0.924, 2.54 (and 0.924, 7.06) for average DC and HD95 on F (and P_n), respectively. MargExc [9] concludes that a single model trained on a single source can not generalized well to other sources based on the results in Table 3 [9]. The Φ_{Fed}^m can surpass Φ_F^m and Φ_{P_n} by a large margin, indicating the strength of ‘bigger data’ from multi-site. That Φ_{Fed}^m has a comparable performance with Φ_{Mix}^m also demonstrate the effectiveness of our multi-site approach. In Table 3, our Φ_{Fed}^m outperforms other centrally trained models [7, 8].

In FL, we can set how many iterations to train on each client before combining parameters to the server. In Table 5, as expected, the fewer iterations on each client before aggregation, the more time-consuming of the overall training. As the Global epoch decreases, the performance of the segmentation model first increases and then decreases. In our experiments, under the same total training iterations, we choose 50 and 2,000 for Client iteration and Global epoch, respectively.

2.2.3 The results of site-adapted model

As mentioned above, we introduce three ways of fine-tuning for site adaptation in each client, thus obtaining three models: (i) Φ_{FTA} , which fine-tunes both the encoder and decoder of the segmentation model; (ii) Φ_{FTB} fine-tunes only the decoder; (iii) Φ_{FTC} fine-tunes only the encoder.

As shown in Table 6, we observe that both Φ_{FTA} and Φ_{FTB} contribute to the performance of the original FL model Φ_{Fed}^m , especially the model Φ_{FTB} . On the dataset F (and P_n), for average DC and HD95, the Φ_{FTB} scheme improves the performance of Φ_{Fed}^m to 0.929, 2.31 (and 0.928, 6.44), respectively. In Table 3, our Φ_{FTB} further approaches to the best non-FL model Φ_{Mix}^m .

Table 6: The segmentation performances of the site-adapted models.

Model	test set	[F] Liver		[F] Spleen		[F] Pancreas		[F] L Kidney		[F] R Kidney		Mean	
		DC	HD95	DC	HD95	DC	HD95	DC	HD95	DC	HD95	DC	HD95
Φ_{Fed}^m	[F&P _{2:5}]	.965	2.41	.939	2.33	.840	4.79	.938	1.65	.936	1.50	.924	2.54
Φ_{FTA}	[F]	.967	1.78	.933	3.25	.840	4.03	.945	1.58	.944	1.43	.925	2.41
Φ_{FTB}	[F]	.969	1.78	.946	2.74	.838	3.97	.946	1.63	.944	1.43	.929	2.31
Φ_{FTC}	[F]	.960	2.22	.925	5.60	.831	4.59	.937	2.06	.938	1.87	.918	3.27

Model	test set	[P ₂] Liver		[P ₃] Spleen		[P ₄] Pancreas		[P ₅] L Kidney		[P ₅] R Kidney		Mean	
		DC	HD95	DC	HD95	DC	HD95	DC	HD95	DC	HD95	DC	HD95
Φ_{Fed}	[F&P _{2:5}]	.938	7.10	.965	1.21	.788	6.99	.966	3.47	.961	16.56	.924	7.06
Φ_{FTA} Φ_{FTB} Φ_{FTC}	[P ₂]	.945	6.55	-	-	-	-	-	-	-	-	-	-
	[P ₂]	.945	6.22	-	-	-	-	-	-	-	-	-	-
	[P ₂]	.938	6.83	-	-	-	-	-	-	-	-	-	-
	[P ₃]	-	-	.965	1.20	-	-	-	-	-	-	-	-
	[P ₃]	-	-	.970	1.14	-	-	-	-	-	-	-	.927
[P ₄]	-	-	.959	1.20	-	-	-	-	-	-	-	.928	6.44
[P ₄]	-	-	-	-	.780	6.71	-	-	-	-	-	.915	6.91
[P ₄]	-	-	-	-	.793	6.50	-	-	-	-	-	-	-
[P ₄]	-	-	-	-	.760	6.88	-	-	-	-	-	-	-
[P ₅]	-	-	-	-	-	-	.974	2.59	.969	16.03	-	-	-
[P ₅]	-	-	-	-	-	-	.972	3.04	.962	15.29	-	-	-
[P ₅]	-	-	-	-	-	-	.963	3.11	.957	16.54	-	-	-

3 Discussion

Clinical practice requires that the learning of organ segmentation models should protect data privacy and can not rely too much on a large amount of fully labeled images, because these annotations are not easy to obtain. In this work, we propose to learn a multi-site multi-organ segmentation model trained on partially labeled datasets from different clinical sites with different target tasks via federated partial supervision. This model aggregates knowledge from all datasets at different sites into a single multi-organ segmentation model, but without any data leakage from each clinical site. Based on this federated learned model with powerful representation capabilities, each clinical site can further adapt this ability to its own needs and applications. We also find the optimal combination of loss functions to maximize knowledge utilization in the PSMOS task, and the model trained by this combination is also considered as our upper bound performance, Φ_{Mix}^m . Extensive experiments have verified the effectiveness of our Federated Partially Supervision method, which can reach the performance of upper bound. In each site, the fine-tuned model can further get a better performance. Our solution can effectively relieve the labeling burden for doctors.

Although our FL model is proven effective compared to the existing methods, it still has several limitations. Our model is trained based on partially labeled datasets belonging to the same region of our body, *i.e.*, abdominal organs. If we want to train a single FL model including more categories of organs from different regions of our body [20], we may encounter the problem that the data distribution varies too much between different sites. This is also a direction we plan to try in the future. Another limitation is that our model training is synchronized between different sites. Every time a new site is added, we must be able to access the data of all past sites at the same time to train a new federated model. There is no data leakage issue, but it is also difficult to access old data from all sites at the same time. Asynchronizing our federated learning is also one of our future research directions, such as through incremental learning [3].

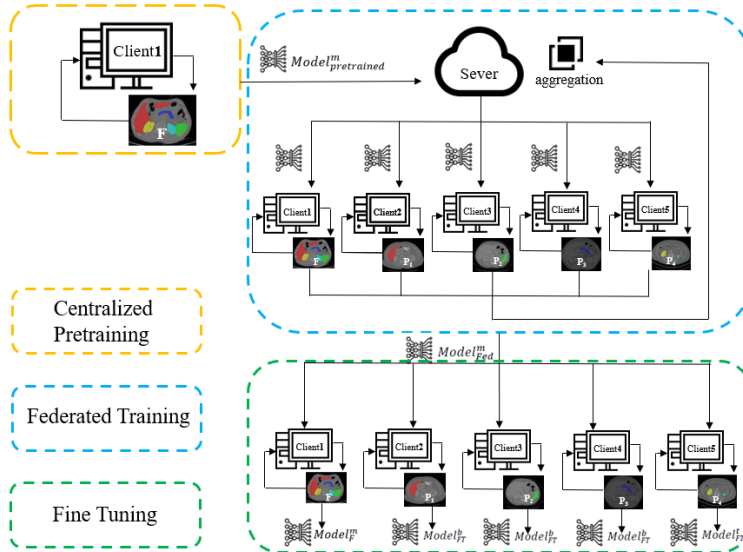


Figure 3: The pipeline of our framework.

4 Materials and Methods

Here we describe the technical details of the FL for the partially supervised multi-organ segmentation and site adaptation approach utilized in this work. The proposed method includes two-stage: (i) Federated aggregation that learns a multi-organ segmentation model from partial supervision, and (ii) Site adaptation that fine-tunes the model with local data to a site-dependent model. Both FL and fine-tuning procedures presented are designed for 3D medical image segmentation tasks. The whole pipeline of our framework is shown in Fig. 3

4.1 Partially supervised multi-organ segmentation (PSMOS)

According to the idea of marginal loss and exclusion loss functions in the literature [9], the marginal loss merges all unlabeled organ pixels into the background label, and the exclusion loss uses the pixels of different organs to be mutually exclusive, that is, a pixel can only belong to a certain organ, but cannot belong to multiple organs. We use a variety of common segmentation loss functions, including Dice Loss [16], Cross Entropy Loss [16], Focal Loss [19], Top-K Loss [18], Lovasz Loss [17], and the combined form of these loss functions, utilizing a small amount of fully annotated data and a large amount of partially annotated data, to train a high-performance multi-organ segmentation neural network in a federated fashion.

For a multi-organ segmentation task with N labels, we define its label set as $\Omega_N = \{C_1, C_2, \dots, C_N\}$. Suppose that a pixel in segmentation belongs a certain class C_n , its label is encoded as a N -dimensional one-hot vector $y'_n = [y_1, y_2, \dots, y_N]$, where $y_n = 1$, otherwise 0. Multi-class classifiers contain a set of response functions $\{f_n(x), n \in \Omega_N\}$, and the posterior classification probability is calculated by the softmax function,

Algorithm 1: FL for partial supervised multi-organ segmentation

Input : number of clients K , FL global rounds R , amount of total training iterations N (n iterations each round), learning rate η
initialize the server model weights: w^0

Output: optimal w^r

```
1 FL Procedure ServerUpdate:
2 for  $r \leftarrow 1$  to  $R$  do
3   for client  $k \leftarrow 1$  to  $K$  do
4      $w_k^{r-1} \leftarrow w^{r-1}$ ;
5      $w_k^r \leftarrow \text{ClientUpdate}(k, w_k^{r-1})$ 
6   end
7    $w^r \leftarrow \sum_{k=1}^K \frac{n_k}{N} w_k^r$ 
8 end

9 Function ClientUpdate ( $k, w_k^{r-1}$ ):
10 for iteration  $i \leftarrow 1$  to  $n$  do
11    $w_k^{r-1,i} \leftarrow w_k^{r-1,i-1} - \eta \nabla l(w_k^{r-1,i-1})$ ;
12 end
13 return  $w_k^r \leftarrow w_k^{r-1,n}$ 
```

$$p_n = \frac{\exp(f_n)}{\sum_{k=1}^N \exp(f_k)}, n \in \Omega_N. \quad (1)$$

4.1.1 Marginal loss

Assume that for images with incomplete segmentation labels, there are only M ($M < N$) labels, its corresponding label index set is Ω'_M . For each merged class label $C_m \in \Omega'_M$, there is a corresponding subset $\Phi_m \subset \Omega_N$. The probability for the merged class m is a marginal probability:

$$q_m = \sum_{n \in \Phi_m} p_n. \quad (2)$$

Also, the one-hot vector for a class m is encoded as $y'_m = [y_1, y_2, \dots, y_M]$. Using the above marginal probability q_m , we define the corresponding marginal loss for Dice loss, cross entropy loss, focal loss,

Top- K loss, and Lovasz loss:

$$L_{Dice}^m = \sum_{m \in \Omega'_M} \left(1 - 2 \cdot \frac{y_m q_m}{y_m + q_m}\right), \quad (3)$$

$$L_{CE}^m = - \sum_{m \in \Omega'_M} y_m \log q_m, \quad (4)$$

$$L_{Focal}^m = - \sum_{m \in \Omega'_M} y_m (1 - q_m)^\gamma \log(q_m), \quad (5)$$

$$L_{Topk}^m(l_Z(f)) = \frac{1}{k} \sum_{i=1}^k L_{CE[i]}^m(f), \quad (6)$$

$$L_{Lovasz}^m = \frac{1}{m} \sum_{m \in \Omega'_M} J(e(m)). \quad (7)$$

In Eq. (5), γ is parameter of focusing, $(1 - q_m)^\gamma$ is a modulation coefficient (we set $\gamma = 2$ in our experiment). In Eq. (6), $L_Z(f) = \{l_i(f)\}_{i=1}^n$, $l_i(f) = l(f(x_i), y_i)$, $l_{[k]}(f)$ is defined as the k th largest element in $l_{[i]}(f)$, we set $k = 10$ in our experiment. In Eq. (7), J is the Lovasz extension of Intersection-over-Union (IoU), and $e(m)$ is the misclassification vector for class m .

4.1.2 Exclusion loss

We define the exclusive subset of class n as E_n , and its label is encoded as a non-one-hot N -dimensional vector $e'_n = [e_1, e_2, \dots, e_N]$, expressed as follows:

$$e'_n = \sum_{k \in E_n} y'_k. \quad (8)$$

The intersection of the prediction p_n of the segmentation network and exclusive label e_n should be as small as possible. Using the above vector e'_n , we define the corresponding exclusion loss for Dice loss, cross entropy loss, focal loss, Top- K loss, and Lovasz loss:

$$L_{Dice}^e = \sum_{n \in \Omega_N} 2 \cdot \frac{e_n p_n}{e_n + p_n}, \quad (9)$$

$$L_{CE}^e = \sum_{n \in \Omega_N} e_n \log(p_n + \varepsilon), \quad (10)$$

$$L_{Focal}^e = \sum_{n \in \Omega_N} e_n (1 - p_n)^\gamma \log(p_n + \varepsilon), \quad (11)$$

$$L_{Topk}^e(l_Z(f)) = - \frac{1}{k} \sum_{i=1}^k L_{CE[i]}^e(f), \quad (12)$$

$$L_{Lovasz}^e = - \frac{1}{n} \sum_{n \in \Omega_N} J(e(n)). \quad (13)$$

In Eqs. (10) and (11), we set $\varepsilon = 1$ to avoid the trap of $-\infty$.

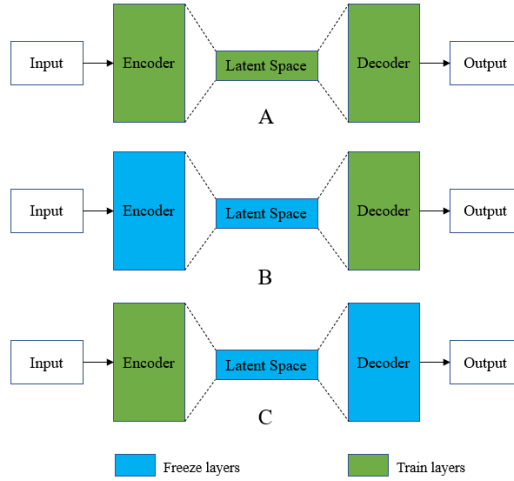


Figure 4: Three different methods of fine-tuning the FL model.

4.2 Federated learning for PSMOS

In our work, the federated learning framework follows the conventional settings as [12], called client-server setup. In the setting, the coordinator is the server that can send the initial model to each client. Then each client trains the same model architecture locally on their data. Once a certain number of clients finish a round of local training, they send the updated model weights or their gradients to the server. The server collects model weights or gradients from clients simultaneously, then aggregates those gradients. After aggregation, the server re-distributes the new weights to the clients, and the next round of local model training begins. This is called one federated training round, the process is repeated until the model converges or the maximum number of iterations is reached. Each client is allowed to select its local best model by monitoring a certain performance metric on a local validation set. The client can select either the global model returning from the server after averaging or any intermediate model considered best during local training based on their validation metric. The definition of FL is as follows, assuming that there are K clients participating in FL, n_k represents the sample numbers of the client k , $n = \sum_{k=1}^K n_k$ represents the total sample numbers of all clients. The goal of FL is to optimize the following objective loss function:

$$\min F(w) := \sum_{k=1}^K \frac{n_k}{n} F_k(w), \quad (14)$$

where w is the parameter that the model needs to learn, and F_k is the local target loss function of client k . In our experiments, we implement the FederatedAveraging algorithm proposed in [12]. The entire FL algorithm for partially supervised multi-organ segmentation is shown in Alg. 1.

In this work, we use a combination of marginal Dice loss, marginal cross entropy loss, marginal Lovasz Loss, exclusion Dice loss, exclusion cross entropy loss, and exclusion Lovasz Loss for a PSMOS task.

4.3 Site adaptation of the FL model

Suppose that the federated model is denoted as Φ_{Fed} , which captures the common task knowledge learned from the aggregated data, the site adaptation module transfers this knowledge from mixed to target site for further improving the performance on the target data domain. Such an adaptation is from a *site-independent* multi-organ segmentation model to a *site-dependent, application-specific* organ segmentation model.

As shown in Fig. 4, we have designed three fine-tuning methods for site adaptation: (i) No freezing. We initialize the target network with the Φ_{Fed} model parameters and fine-tune the entire neural network. (ii) Freezing encoder. We initialize the target network with the parameters of the Φ_{Fed} model, freeze the encoder, and fine-tune the decoder part of the network. (iii) Freezing decoder. We initialize with the parameters of the Φ_{Fed} model, freeze the decoder, and fine-tune the encoder part of the network.

References

- [1] B. Van Ginneken, C. M. Schaefer-Prokop, and M. Prokop, “Computer-aided diagnosis: How to move from the laboratory to the clinic,” *Radiology*, vol. 261, no. 3, pp. 719–732, 2011.
- [2] J. Sykes, *Reflections on the current status of commercial automated segmentation systems in clinical practice*, 2014.
- [3] P. Liu, X. Wang, M. Fan, H. Pan, M. Yin, X. Zhu, D. Du, X. Zhao, L. Xiao, L. Ding, *et al.*, “Learning incrementally to segment multiple organs in a ct image,” in *Medical Image Computing and Computer Assisted Intervention—MICCAI 2022: 25th International Conference, Singapore, September 18–22, 2022, Proceedings, Part IV*, Springer, 2022, pp. 714–724.
- [4] S. Chen, K. Ma, and Y. Zheng, “Med3d: Transfer learning for 3d medical image analysis,” *arXiv preprint arXiv:1904.00625*, 2019.
- [5] R. Huang, Y. Zheng, Z. Hu, S. Zhang, and H. Li, “Multi-organ segmentation via co-training weight-averaged models from few-organ datasets,” in *International Conference on Medical Image Computing and Computer-Assisted Intervention*, Springer, 2020, pp. 146–155.
- [6] K. Dmitriev and A. E. Kaufman, “Learning multi-class segmentations from single-class datasets,” in *Proceedings of the IEEE/CVF Conference on Computer Vision and Pattern Recognition*, 2019, pp. 9501–9511.
- [7] Y. Zhou, Z. Li, S. Bai, C. Wang, X. Chen, M. Han, E. Fishman, and A. L. Yuille, “Prior-aware neural network for partially-supervised multi-organ segmentation,” in *Proceedings of the IEEE/CVF International Conference on Computer Vision*, 2019, pp. 10 672–10 681.
- [8] X. Fang and P. Yan, “Multi-organ segmentation over partially labeled datasets with multi-scale feature abstraction,” *IEEE Transactions on Medical Imaging*, vol. 39, no. 11, pp. 3619–3629, 2020.
- [9] G. Shi, L. Xiao, Y. Chen, and S. K. Zhou, “Marginal loss and exclusion loss for partially supervised multi-organ segmentation,” *Medical Image Analysis*, vol. 70, p. 101 979, 2021.

- [10] J. Zhang, Y. Xie, Y. Xia, and C. Shen, “Dodnet: Learning to segment multi-organ and tumors from multiple partially labeled datasets,” in *Proceedings of the IEEE/CVF Conference on Computer Vision and Pattern Recognition*, 2021, pp. 1195–1204.
- [11] Q. Yang, Y. Liu, T. Chen, and Y. Tong, “Federated machine learning: Concept and applications,” *ACM Transactions on Intelligent Systems and Technology (TIST)*, vol. 10, no. 2, pp. 1–19, 2019.
- [12] B. McMahan, E. Moore, D. Ramage, S. Hampson, and B. A. y Arcas, “Communication-efficient learning of deep networks from decentralized data,” in *Artificial intelligence and statistics*, PMLR, 2017, pp. 1273–1282.
- [13] X. Xu and P. Yan, “Federated multi-organ segmentation with partially labeled data,” *arXiv preprint arXiv:2206.07156*, 2022.
- [14] C. Shen, P. Wang, D. Yang, D. Xu, M. Oda, P.-T. Chen, K.-L. Liu, W.-C. Liao, C.-S. Fuh, K. Mori, *et al.*, “Joint multi organ and tumor segmentation from partial labels using federated learning,” in *Distributed, Collaborative, and Federated Learning, and Affordable AI and Healthcare for Resource Diverse Global Health: Third MICCAI Workshop, DeCaF 2022, and Second MICCAI Workshop, FAIR 2022, Held in Conjunction with MICCAI 2022, Singapore, September 18 and 22, 2022, Proceedings*, Springer, 2022, pp. 58–67.
- [15] F. Isensee, P. F. Jaeger, S. A. Kohl, J. Petersen, and K. H. Maier-Hein, “Nnu-net: A self-configuring method for deep learning-based biomedical image segmentation,” *Nature methods*, vol. 18, no. 2, pp. 203–211, 2021.
- [16] J. Long, E. Shelhamer, and T. Darrell, “Fully convolutional networks for semantic segmentation,” in *Proceedings of the IEEE conference on computer vision and pattern recognition*, 2015, pp. 3431–3440.
- [17] M. Berman, A. R. Triki, and M. B. Blaschko, “The lovász-softmax loss: A tractable surrogate for the optimization of the intersection-over-union measure in neural networks,” in *Proceedings of the IEEE conference on computer vision and pattern recognition*, 2018, pp. 4413–4421.
- [18] Y. Fan, S. Lyu, Y. Ying, and B. Hu, “Learning with average top-k loss,” *Advances in neural information processing systems*, vol. 30, 2017.
- [19] T.-Y. Lin, P. Goyal, R. Girshick, K. He, and P. Dollár, “Focal loss for dense object detection,” in *Proceedings of the IEEE international conference on computer vision*, 2017, pp. 2980–2988.
- [20] P. Liu, Y. Deng, C. Wang, Y. Hui, Q. Li, J. Li, S. Luo, M. Sun, Q. Quan, S. Yang, *et al.*, “Universal segmentation of 33 anatomies,” *arXiv preprint arXiv:2203.02098*, 2022.